Near-surface turbulence for evaporative convection at an air/water interface

K. A. Flack
Department of Mechanical Engineering, United States Naval Academy, Annapolis, Maryland 21402

J. R. Saylor[a] and G. B. Smith
Naval Research Laboratory, Washington, DC 20375

(Received 3 November 2000; accepted 22 August 2001)

Turbulence measurements are reported for the flow beneath an air/water interface undergoing evaporative convection. Measurements were obtained using a two component laser Doppler velocimeter system. Two hydrodynamic boundary conditions were considered for the free surface: a shear free surface, which is the case when surfactants are absent, and a constant elasticity surface, created by depositing a monolayer of oleyl alcohol. The shear free boundary condition case results in significantly higher levels of near surface turbulence than the constant elasticity case. This difference between the two cases decreases with distance from the free surface. Profiles of the turbulent fluctuations were obtained for the horizontal and vertical velocity components and are compared with the somewhat analogous case of a heated solid wall. [DOI: 10.1063/1.1410126]

I. INTRODUCTION

The study of natural convection is driven by its relevancy to a wide spectrum of fluid flows, ranging from geophysical flows in meteorology and oceanography, to technologically relevant flows in heating, ventilation, and air conditioning (HVAC) and chemical processing applications. Most research on natural convection addresses the heat transfer and fluid mechanics that occur in a layer of fluid contained between a solid upper and lower boundary. The thermal boundary condition for the upper and lower plates are of either the constant temperature or constant heat flux type while the hydrodynamic boundary condition is of the no-slip type for both boundaries.

In contrast to this solid-wall model of natural convection, many environmentally relevant flows involve a free surface. Hence, natural convection occurs in an environment where the no-slip boundary condition does not apply to the surface at which heat transfer occurs. In oceanographic applications, for example, heat transfer occurs at the air/sea interface, where the no-slip boundary condition does not apply. Similarly, in meteorology convective cells form within layers of the atmosphere where either the upper or lower boundary condition is of the no-slip type.[1]

In this study, we focus on evaporative convection, which is natural convection in a layer of liquid, driven by evaporation at a free surface. Evaporative convection is relevant to oceanography and limnology, where evaporation at the air/water interface can drive natural convection in the water bulk. For these flows, the no-slip boundary condition does not apply. Rather, for this natural convection paradigm, the free surface has a shear-free hydrodynamic boundary condition when the water surface is free of surfactant monolayers and a constant elasticity boundary condition when surfactant monolayers are present. As will be demonstrated in this paper, the difference in these three boundary conditions: (i) no-slip, (ii) shear-free, and (iii) constant elasticity, is important and has a significant effect on the hydrodynamics that occur in the near-surface region.

Of particular interest in the present work are the profiles of the fluctuating components of velocity in directions normal and parallel to the water surface, w' and u', respectively. The effect of the differing boundary conditions may be seen in the structure of the turbulence near the interface. Such measurements have been studied in great detail for the case of a solid wall. Perhaps the earliest solid wall studies are due to Thomas and Townsend,[2,3] who performed detailed measurements of the fluctuating components of velocity as a function of the distance from a heated plate. The literature published since these early studies is large and an adequate discussion of all the relevant references is beyond the scope of this work. An excellent review can be found in Adrian *et al.*[4] Noteworthy investigations in this area include the work of Deardorff and Willis,[5] Wyngaard, *et al.*,[6] and Sorbjan.[7]

The u' and w' velocity profiles for the solid wall case tend to have the following form. For u', the profile has a value of zero at the wall and rises quickly to a peak very close to the wall. The profile then drops slightly and remains relatively constant for most of the region between the two solid plates. For w', the profile is essentially symmetric about the midplane, gradually rising from zero and asymptoting to a constant value near the midplane. The u' and w' profiles are a function of heat flux and distance between the solid plates. However, by introducing appropriate scaling parameters for velocity and z, the profiles of u' and w' can be made independent of tank size and heat flux (or Rayleigh number). Following the treatment presented in Adrian *et al.*,[4] these scales are z_* and w_*, where z_* is the tank depth, and w_* is defined as

[a]Current address: Clemson University, Clemson, South Carolina 29634.

$$w_* = (\beta g Q_0 z_*)^{1/3}, \tag{1}$$

$$Q_o = q''/\rho c_p, \tag{2}$$

where q'' is the heat flux through the surface, β is the thermal coefficient of expansion, ρ is the density of the working fluid, c_p is the specific heat, and g is gravity. Due to evaporative cooling, the temperature of the working fluid decreased continuously resulting in a varying heat flux during the course of a run. To compare data from different heat fluxes on the same plot, this above scaling was used to collapse our data. We do not expect our collapsed data to agree with that of solid wall studies, due to the difference in boundary conditions. However, the scaling is appropriate since it is the same type of turbulence, namely buoyancy-driven turbulence.

Initial work in the area of evaporative convection consisted of flow visualizations. For example, the general studies of Spangenberg and Rowland[8] used schlieren photography of evaporative convection in a glass water tank, and observed the formation of cold lines on the water surface, which resulted in plunging sheetlike structures in the liquid bulk. Katsaros *et al.*[9] performed flow visualizations using Kalliroscope particles, in a 0.75 m by 0.50 m by 0.5 m Plexiglas water tank illustrating, in a more direct fashion, the plunging sheets of fluid. Chernous'ko[10] visualized the flow induced in water during evaporative convection by sprinkling dye particles on the water surface and observing their evolution. Plunging sheets were observed in addition to spiral vortices, both of which entrained the dye into the liquid bulk.

A significant body of evaporative convection research addresses the bulk relationships between fluid flow and heat transfer. For example relationships between the rate of heat transfer from the water surface and the characteristics of the air flow above the water surface (via the air-side Rayleigh number or Reynolds number) were developed by Sharpley and Boelter,[11] Boelter *et al.*,[12] and Sparrow and co-workers.[13–17] While not directly relevant to the present work, it is noted that the air-side flow plays an important role in ascertaining the heat flux from the water surface.

With regard to measurements of velocity during evaporative convection, the only existing study is that of Volino and Smith,[18] who simultaneously recorded the surface temperature field and subsurface velocity field using infrared imaging and particle image velocimetry (PIV), respectively. In this work, the existence of both falling sheets and spiral vortices were quantitatively confirmed in the velocity fields that were obtained in planes parallel and perpendicular to the free surface. Profiles of u' or w' were not obtained in this work, and a quantification of the role of surfactants was not obtained.

In the current work, profiles of u' and w' are obtained for evaporative convection. These experiments are conducted for surfaces free of surfactant monolayers, and for a surface with a known concentration of surfactant. As such, these experiments provide two results that have not been obtained heretofore. First, these are the first u', w' profiles obtained in an evaporative convection flow. Second, this is the first study that quantifies the effect of changing hydrodynamic boundary conditions on subsurface hydrodynamics; namely, the difference between no-slip, shear-free, and constant elasticity boundary conditions is revealed.

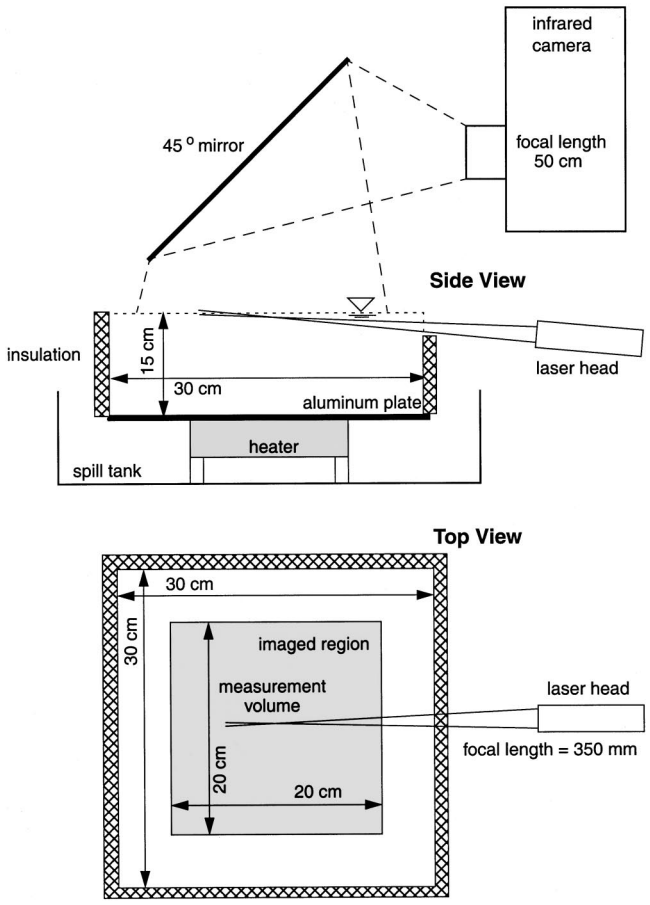

FIG. 1. Experimental configuration.

II. EXPERIMENTAL APPARATUS AND CONFIGURATION

The experiments were performed in a water tank at the United States Naval Academy Fluids Laboratory. The dimensions of the tank are $15\,\text{cm} \times 30\,\text{cm} \times 30\,\text{cm}$, as shown in Fig. 1. The tank is constructed of 3.2 mm thick glass within an aluminum frame. RTV silicon was used to seal the tank. Polystyrene foam (2.5 cm thick; $R=5$) was attached to the tank walls to minimize heat loss. The base of the tank sat on an electrical heater, which was used to elevate the initial bulk temperature of the tank water. An aluminum base plate, attached to the tank bottom, was used to distribute the heat flux more uniformly, thereby protecting the glass from thermal stresses.

The water source for the experiments was a Milli-Q UV Plus system, which has an upstream single deionization still and downstream millipore and ultraviolet (UV) filters. A ten gallon Nalgene carboy served as the supply reservoir and was connected to the tank by teflon tubing and fittings. Silicon sealant was used to seal the tubing and fittings. The water tank was gravity fed from the carboy through a hole in the tank bottom. Water was taken from the bottom of the

reservoir to avoid the introduction of any surfactant that accumulated on the surface of the reservoir. Great care was taken to ensure the water in the tank was free of contaminants and surfactants. Once the water was obtained from the Milli-Q UV system, the deionized water only came in contact with a Nalgene carboy, teflon tubing, silicon sealant, the glass tank, glass rods for swiping the surface, and a glass thermometer. Prior to filling, the tank was cleaned with methanol and rinsed numerous times with deionized water. The tank was then soaked for 24–48 h with deionized water before the initial filling to leach any surface active material from the seals and surfaces. Further cleaning procedures performed prior to each test run included overfilling the tank by approximately the volume of the tank, sparging with N_2 bubbles introduced by a glass frit to scavenge the surfactant from the bulk, and frequent swiping of the surface with a glass rod cleaned with methanol and rinsed with deionized water.

In addition to careful cleaning procedures, it is also important to have a means for monitoring surface cleanliness, since a clean surface can become contaminated without any change that is visible to the naked eye. Surface cleanliness is typically monitored using an *in situ* surface tension measurement device such as a Wilhelmy plate. Separate experiments[19] have revealed that dramatic changes in IR imagery can occur upon contamination of a clean surface, accompanied by a barely discernible change in surface tension, as measured via a Wilhelmy plate. These measurements indicate that the IR imagery is a more sensitive indicator of contamination (albeit a more qualitative one) than traditional surface tension measurements. In the current work, the water surface was monitored with the IR camera while the velocity measurements were obtained to ensure that the surfactant-free results were not contaminated.

Before each test the tank was slowly overfilled with water from the reservoir while being heated from below. Surface contaminants, as determined from the infrared imagery, were swiped off throughout the overfilling/heating process. Once the surface was determined to be clean and the water was approximately 20 °C above the ambient room temperature, the heater was turned off. The heater plate was then allowed to cool for a period of approximately 45 min. Tests were performed once the temperature of the air gap between the aluminum baseplate and the glass tank (obtained with a thermocouple) was equal to the bulk water temperature. This ensured that buoyant plumes of warm fluid were not forming at the tank floor. When this procedure was completed, the bulk water temperature was typically 14 °C–16 °C above the ambient room temperature.

Two surface conditions were considered for these experiments. The first was a clean condition, achieved using the cleaning procedure described above. The second condition was a surfactant case, achieved by depositing 10 μl of a stock solution of oleyl alcohol in HPLC grade heptane using a micrometer syringe. The stock solution was 9.9 μg/μl of heptane and the resulting surfactant concentration on the water surface was 0.11 μg/cm^2. The selection of oleyl alcohol as the surfactant was based on previous experiments that determined that it did not impede the evaporation at the surface.[20,21] At the concentration used here, oleyl alcohol creates a surface pressure of 19 mN/m, as determined by the data of Barger.[22]

Infrared images of the water surface were obtained using a Raytheon-Amber AE4256 CCD camera containing a 256 $\times$254 InSb array. The camera is liquid nitrogen cooled and exhibits a noise level of 25 mK in measured temperature at each pixel. The camera viewed the water surface via a 45° mirror. The imaged footprint was about 16 cm on a side, centered within the tank. The pixel intensity output from the camera was converted to temperature using a two step calibration procedure, as outlined in Saylor *et al.*,[23,24] which resulted in a temperature error of less than 0.25%. A length scale calibration was also performed to determine the actual size of the imaged structures. This was accomplished by imaging a ruler to compute a length-per-pixel value.

Two components of velocity were obtained with a TSI ColorBurst system with a 4 W argon-ion laser. One fiber-optic probe contains all four beams along with the transmitting and receiving optics for backscatter data acquisition. A 350 mm lens was used on the probe resulting in a measuring volume length of 2.3 mm and diameter of 0.16 mm. The blue (486 mm) and green (514.5 mm) beams were rotated 45°. This orientation required coincidence data acquisition, having a coincidence window of 0.01 s. In order to obtain measurements very near the free surface, the probe was tilted upward approximately 5°, resulting in one blue and one green beam nearly parallel to the water surface. Since the tank was filled to the point of having a meniscus, the beams were tilted at a slightly higher angle than surface parallel in order to transmit the beams through the glass without distortion due to the meniscus. Tilting the beams incurred a fixed error of less than 0.5% to the velocity measurements.

III. DATA ACQUISITION AND DATA REDUCTION

The bulk water temperature in the tank was measured throughout the experiment with mercury in a glass thermometer, having 0.1 °C resolution. The rate of decrease in temperature was used to compute the total heat loss from the water. This heat loss is due to evaporation at the surface as well as conduction through the sides and base of the tank. In order to quantify the conductive heat loss, an additional experiment was performed at the same ambient conditions. The tank was heated to 20 °C above ambient, and then capped with a 48 mm Plexiglas lid with an additional 10 cm of insulation to essentially eliminate heat transfer through the top of the tank. The bulk water temperature was then recorded over a period of 12 h, yielding the conductive heat loss (approximately 25% of heat flux due to evaporation). This loss was used to correct the evaporative heat flux data provided in Sec. IV.

The measurement volume was traversed in the surface normal direction using a Velmex 9800 traverse with a resolution of 5 μm. The 5° tilted beams allowed for accurate detection of the surface. The surface was initially located visually by positioning the center of the measurement volume at the point where the beams refract at the surface. Fine adjustments were then made by observing the quality of the

TABLE I. Heat flux, convective velocity, and Reynolds number range for each run.

	q''(W/m^2)	w_*(mm/s)	$\mathrm{Re}_*=w_*z_*/\nu$
Run 1—Clean	498–348	4.0–3.5	860–690
Run 2—Clean	560–345	4.2–3.5	890–690
Run 1—Surfactant	375–283	3.6–3.3	780–642
Run 2—Surfactant	372–259	3.6–3.2	780–620

laser Doppler velocimeter (LDV) signal as the measurement volume approached the surface. This method locates the position of the free surface within approximately one measurement volume diameter. At the end of each profile, the free surface was relocated, accounting for any change in surface level during the experiment. Evaporation in the tank resulted in a surface level change of approximately 6 μm/min (total run times were approximately 90 min), an amount that would not significantly affect the initial readings very near the surface.

To obtain velocity profiles, the measurement volume was moved to the first location and data was obtained. The measurement volume was then traversed to each subsequent location in the profile. Velocity profiles were obtained at 15 vertical depths in the tank ranging from 0.2 to 50 mm below the surface. For one run, data was first taken near the surface and then the measurement volume was traversed downward from the surface. The heat flux decreased as the measurement volume moved away from the surface since the bulk water temperature decreased over the 90 min that the velocity profile was obtained. The second data run was taken first in the bulk water, 50 mm below the surface, and then the measurement volume was traversed upward toward the surface, frequently relocating the free surface. For this case, the heat flux decreased as the measurement volume moved toward the surface. Table I lists the range of heat flux, convective velocity, and Reynolds number based on convective scales during each run.

The water was seeded with TiO_2 particles, approximately 2–4 μm in diameter. The cleanliness of the particles was a concern since any surfactant on the particles would be difficult to remove from the bulk water. The particles were cleaned by a rigorous, multistep process. Initially the particles were soaked in deionized water. The particles accumulated at the bottom of the container and the surfactant, which rose to the surface, was decanted off. This process was repeated several times. The soaking and decanting process was then repeated several times with methanol and then heptane. Particle cleanliness was tested by monitoring a clean water surface with the IR camera while depositing some of the particles on the water. There was no discernable difference between the infrared image obtained before and after the inclusion of the cleaned TiO_2 particles.

High data rates proved challenging due to the very low velocities observed during the experiments. Velocities were on the order of 3–6 mm/s with a zero average velocity for both components. The fringes were shifted at 5 kHz to remove directional ambiguity. The fringe velocity of approximately 18 mm/s resulted in multiple readings of slow moving particles in the measurement volume. The repeated validations for a particle that remained for long periods in the measurement volume were filtered from the data based on a minimum time between valid bursts, prior to statistical analysis.

Data at each depth was obtained over a period of 10 min, resulting in 2000–3000 valid data points. The measurements from the experiments at like conditions (measurement volume traversing away from the surface and toward the surface) were averaged once nondimensionalized by the heat flux, resulting in datasets consisting of 4000–6000 data points. The total fixed and precision errors based on a 95% confidence interval for the turbulence data is less than 5% for both components.

IV. RESULTS

Surface temperature and subsurface turbulence measurements of an air water interface undergoing evaporative convection are now presented. Figures 2(a) and 2(b) show infrared images of clean and surfactant covered surfaces, respectively, for a heat flux of 407 W/m^2. In both images, the average temperature has been subtracted, so that white represents temperatures above the average and black represents temperatures below the average. The dynamic range of the image is approximately 1 K. As seen in the figures, there is a dramatic change in spatial scale of the convective structure when comparing the clean and surfactant cases. The clean surface shows a large range of scales, including very fine structures, the smallest of which may not be captured due to the spatial resolution limit of the camera. In contrast, the surfactant case exhibits much larger-scale structures, some of which are vortical in nature. Observing the images in real time reveals structures in the clean case that are highly active as the warm fluid (white) rises to the surface and falls rapidly in thin cool sheets (black). By comparison, the structures in the surfactant case are much less active, remaining coherent for much longer time periods. A more complete description of the infrared images, including statistics on the temperature fields, is found in Saylor *et al.*[23,24]

The spatial and temporal differences observed in the temperature fields are obviously linked to the near-surface convective turbulence. This is confirmed in Figs. 3 and 4, where sample time traces are presented for the horizontal (U) and vertical (W) component of velocity for the clean and surfactant cases at two near-surface depths. The data presented was obtained over a period of 200 s. Gaps in the time trace for the surfactant data indicate periods of zero data rate. Low data rate, inherent to very low-velocity flows, were more common for the less active surfactant case.

For the very near-surface case (Fig. 3), marked differences are apparent between the clean and surfactant cases. Looking first at the horizontal velocity traces, note the dramatic reduction in the highest-frequency fluctuations of the signals, with the addition of the surfactant. The clean signal also appears to include a large-amplitude, low-frequency structure that is also damped by the addition of surfactant to the surface. The vertical velocity fluctuations are much smaller than the horizontal for both the clean and surfactant

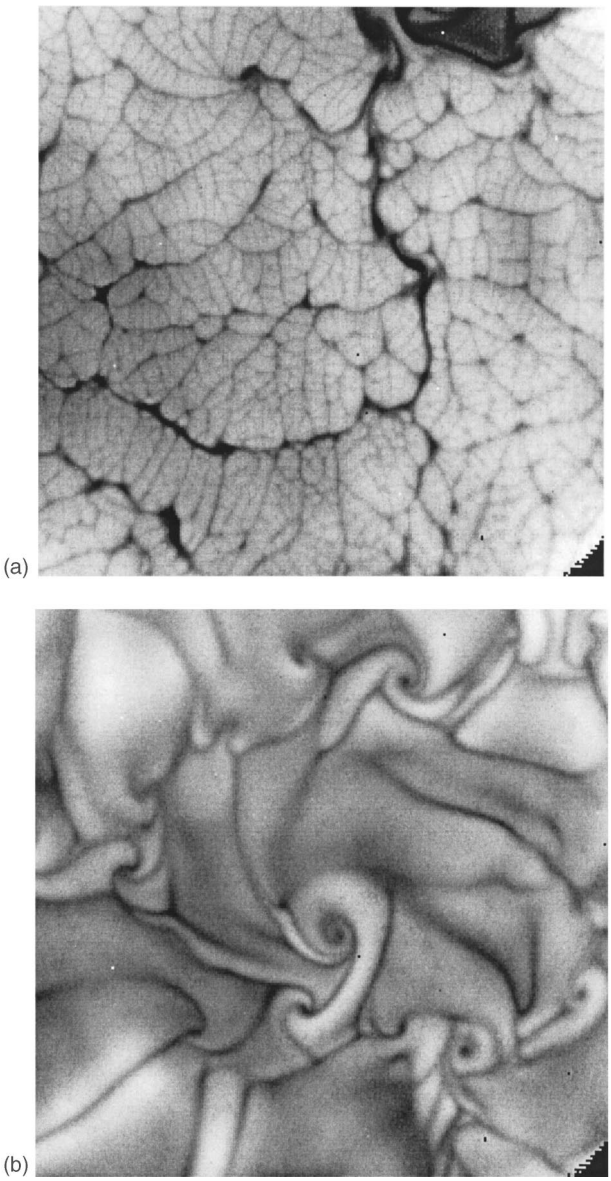

FIG. 2. (a) Infrared image clean surface, $q''=407\ \mathrm{W/m^2}$. (b) Infrared image surfactant surface, $q''=407\ \mathrm{W/m^2}$.

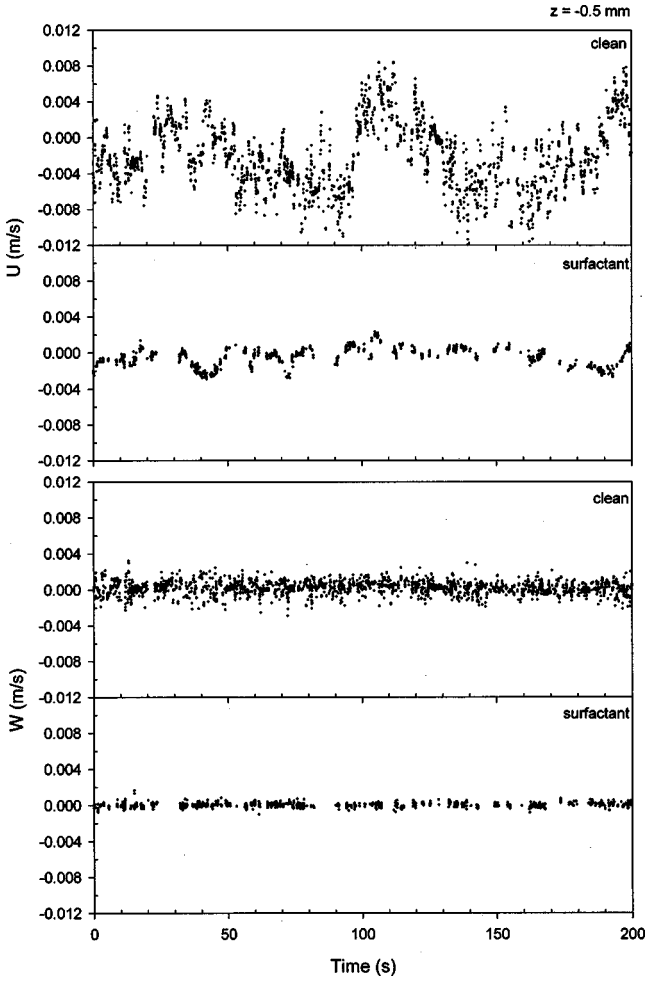

FIG. 3. Velocity time trace, $z=-0.5$ mm.

cases. This is expected due to the zero vertical velocity boundary condition at the interface. There does not appear to be a damping of high-frequency fluctuations due to the addition of the surfactant, for the vertical velocity.

At a depth of 4 mm (Fig. 4), the differences between the clean and surfactant cases are much less pronounced. The traces for the horizontal velocity component are qualitatively almost identical for the clean and surfactant runs, with the exception of a slight damping in the vertical velocity component for the surfactant case. As the distance from the surface increases, there is a reduction in the high-frequency fluctuations and an overall reduction in the horizontal velocity magnitudes for the clean case. This indicates that the intense fluctuations in the horizontal plane are confined to a very thin (<4 mm) surface sublayer.

The observations discussed above are quantified in the turbulence profiles presented in Fig. 5. The horizontal (u') and vertical (w') components of the turbulence intensities have been nondimensionalized by convection scales [Eqs. (1), (2)]. As discussed in the data acquisition section, the data were obtained during two different runs. These runs provided identical points at two heat fluxes. An examination of the separate runs showed some scatter, even with the convection scaling. However, the scatter is significantly less than the differences due to changes in the boundary condition. Based on the convection scaling, we make the assumption that the heat flux dependence has been removed from the data. This allowed averaging the data from the two runs, thereby reducing the noise in the averaged data presented in Fig. 5.

Note that the data collapses below a certain depth for the two different boundary conditions. This suggests that the assumption of the validity of the convection scaling is correct at these depths, and that the effect of the boundary is not felt at this depth. The differences near the surface are most likely due to differences in the free surface boundary condition.

The high level of turbulent activity near the surface for the shear free boundary condition (clean) is evident in Figs. 5(a) and 5(b) when compared to the constant elasticity boundary condition (surfactant). The horizontal component of the turbulence intensity [Fig. 5(a)] is four to five times larger near the surface for the clean case than for the surfactant case. Both cases reach approximately the same level of u at $z/z_*=0.1$, or 15 mm below the surface. The turbulence

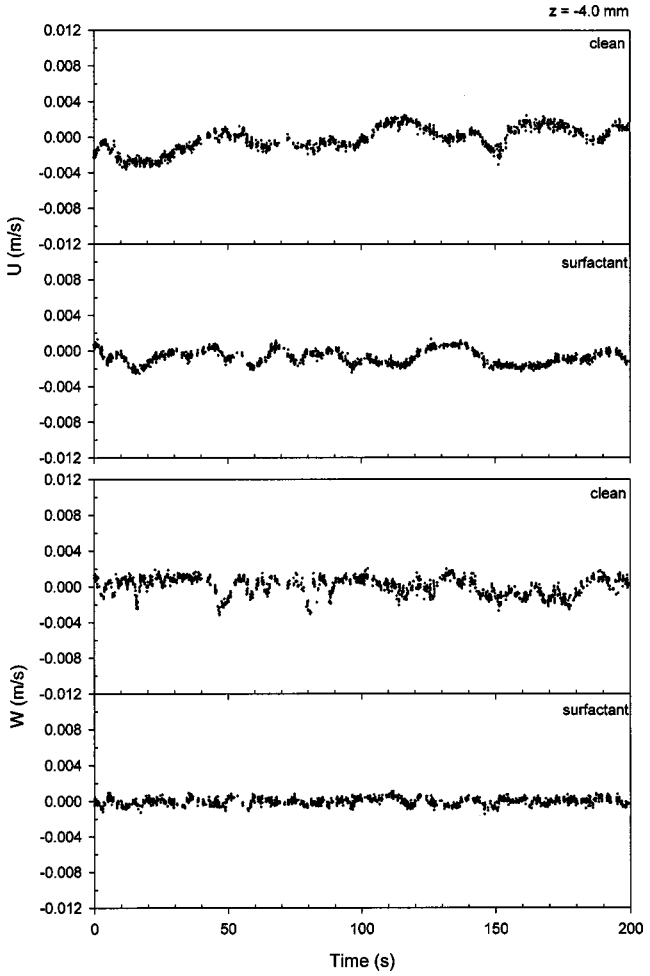

FIG. 4. Velocity time trace, $z=-4$ mm.

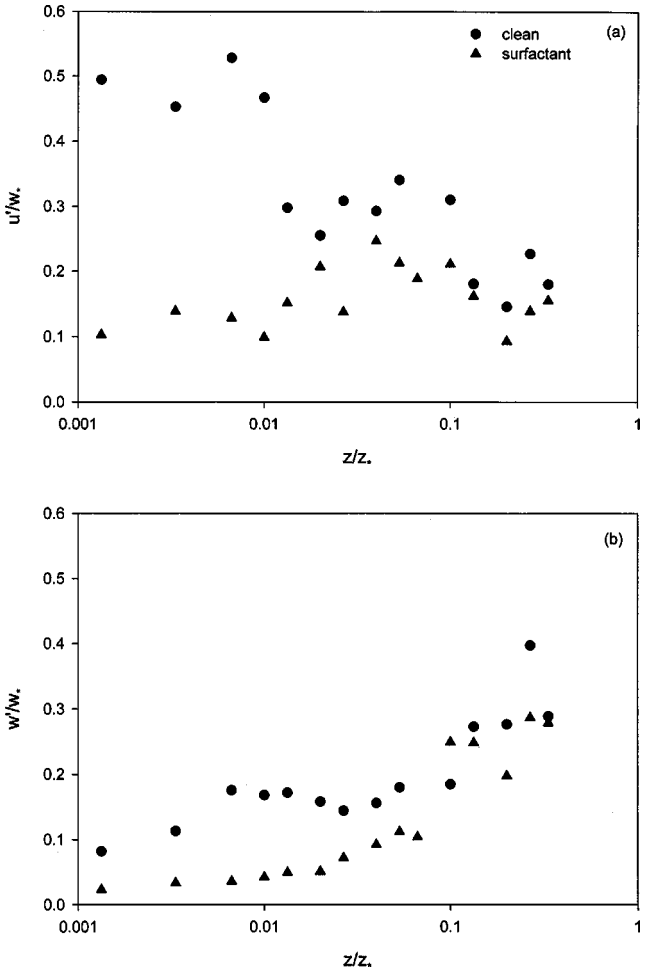

FIG. 5. The rms velocity profiles, clean and surfactant.

intensity in the vertical direction [Fig. 5(b)] is also significantly larger (three to four times) for the clean case than the surfactant case near the surface, before approaching the same level approximately 15 mm ($z/z_*=0.1$) below the surface. These results reveal that changing the hydrodynamic boundary condition from shear-free to constant elasticity changes the turbulence intensity by as much as a factor of 5. This difference is confined to a thin sublayer, approximately $0.1z_*$ in extent.

V. DISCUSSION

The primary result obtained from the experiments herein concerns the difference between clean and surfactant behavior, particularly near the water surface. The differences between the shear-free, constant elasticity and no-slip boundary conditions are now further explored by comparing the turbulence results of the present experiment to two natural convection experiments, where turbulence measurements were obtained in the horizontal layer above a heated surface with an insulated top. For the heated wall studies there is a no-slip boundary condition at the boundary where heat transfer occurs, compared to the shear-free or constant elasticity boundary for the present experiment, as illustrated in Fig. 6. Turbulence results from all three experiments are presented in Figs. 7(a) and 7(b). The turbulence measurements of Prasad and Gonuguntla[25] were obtained with a planar particle image velocimeter (PIV) system, whereas the results of Adrian *et al.*[4] were obtained with a two-component LDV system. All data has been nondimensionalized using convection scales. The kinematic heat flux, $Q_0=q'/\rho c_p$, from the heated surface was 0.15 °C mm/s for Adrian and $Q_0=0.20$ °C mm/s for Prasad. For the present experiments, Q_0 ranged from 0.06–0.12 °C mm/s.

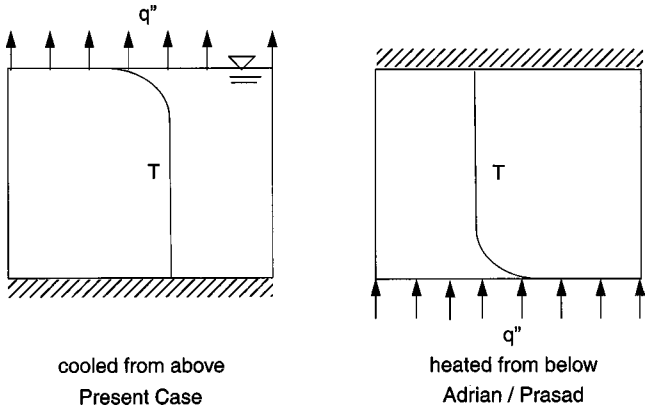

FIG. 6. A comparison of experimental configurations.

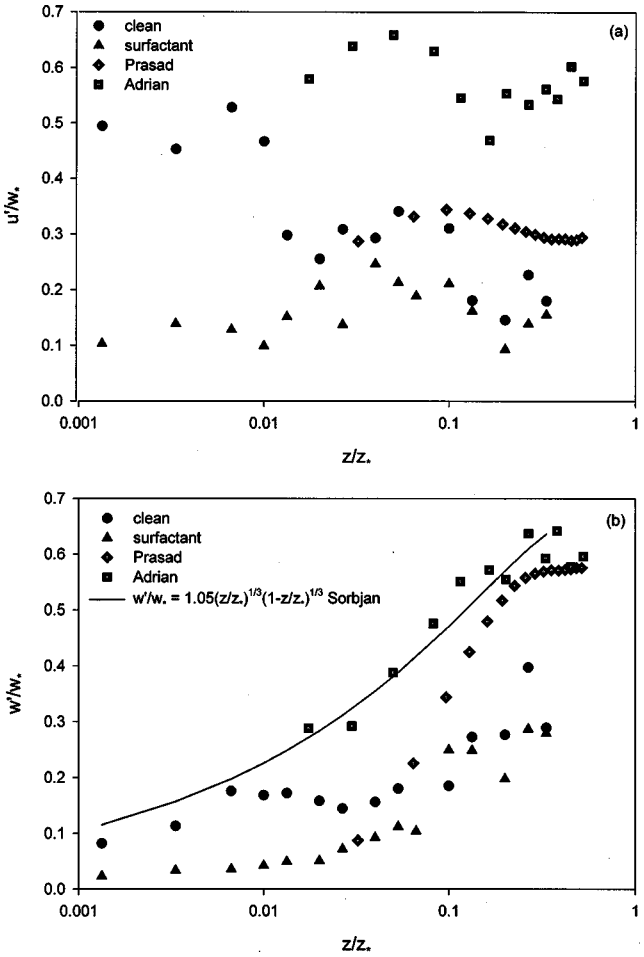

FIG. 7. The rms velocity profiles, clean and surfactant.

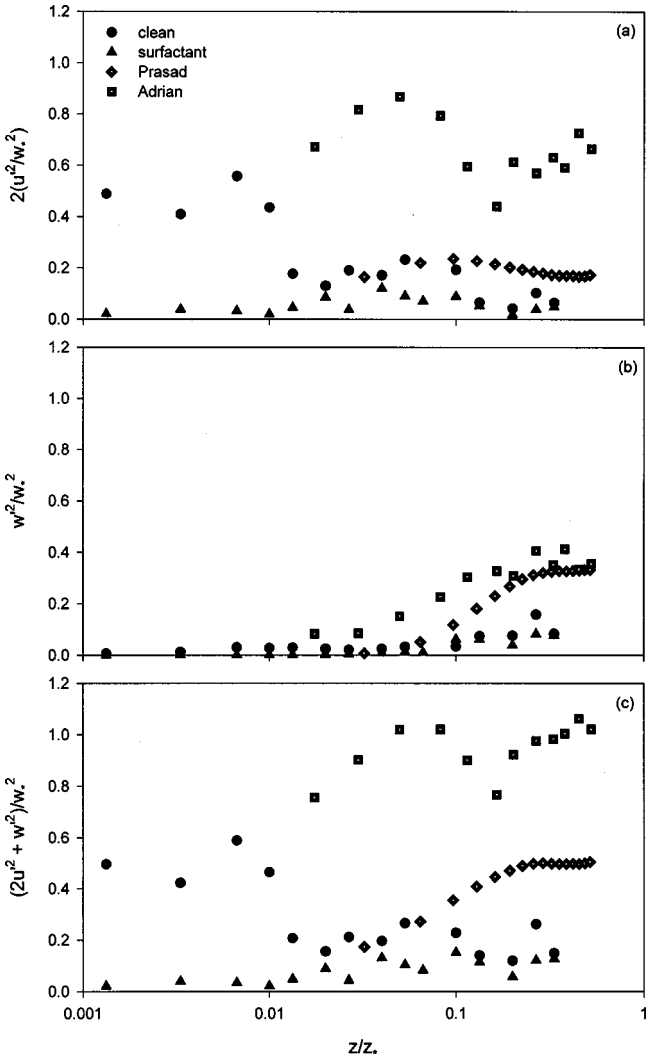

FIG. 8. Kinetic energy.

In Fig. 7(a) the scaled u' data from the present experiments are presented, along with that due to Prasad *et al.* and Adrian *et al.* It is noted that the data from the present clean and surfactant experiments extends down to a value of $z/z^* \sim 0.001$. Unfortunately, the data of both Prasad and Adrian do not extend to values of $z/z^* < 0.01$, making comparisons somewhat difficult. Some comparison can be made, however, since it is known that for the solid wall studies of Prasad and Adrian, the u' data must approach zero in this region. In contradistinction to this solid wall behavior, for the data presented here (particularly for the clean case) the values of u' are relatively large. Indeed, for the clean case, the value of u' reaches its maximum at the smallest value of z/z^* measured. This is an important difference between the free surface and solid wall studies. Moreover, observing the results of Prasad and Adrian, it seems that u' reaches a peak at a location relatively deep in the water bulk, indicating that the turbulent kinetic energy is necessarily expressing itself away from the wall, where it is not damped by the wall. Again, in contrast to this solid wall behavior, the clean case shows its maximum right at the surface, since this region experiences the least amount of resistance or damping. This point is further borne out in Figs. 8(a) and 8(c), where data for the u component of turbulent kinetic energy (TKE) and total TKE are presented, respectively. Here again, the clean data shows its maximum value at the surface, while the solid wall cases show a maximum deeper in the bulk.

For all cases discussed here (solid wall, constant elasticity, and shear-free), w' must equal zero at $z/z^* = 0$. This trend is observed in Fig. 7(b), where all four datasets approach a value of zero as z/z^* decreases (a theoretical similarity equation by Sorbjan[7] with a constant based on the Adrian data is included). As z/z^* increases, w' increases for all cases plotted. This trend is expected, since w' must achieve large values away from either the solid wall or the free surface, and hence gets larger as one travels into the water bulk. This trend is also observed in Fig. 8(b), for the vertical component of TKE.

For the u' and w' data of Fig. 7 and for the TKE plots of Fig. 8, the ''deep water'' (large z/z^*) behavior of the Prasad and Adrian data significantly exceed the values of the present data. Moreover, there is also a significant difference in the values obtained by Prasad and Adrian over the entire range of z/z^*. The exact cause of these disparities is unclear. The differences may be due to an inability of the scaling parameters to collapse this data. The difference may also also be due to differences in the measurement methods for all three

experiments. Accordingly, in the aforementioned discussion, we have focused on changes in the velocity or TKE data as a function of z/z^*, rather than absolute values for these parameters.

VI. CONCLUSIONS

Significant differences are observed for the subsurface hydrodynamics during evaporative convection depending on the surface boundary condition. A shear-free boundary shows a higher level of near-surface turbulence compared to a constant elasticity boundary condition. This difference is largest in the horizontal component of velocity and is contained in a thin near-surface sublayer. The solid wall boundary condition displays higher levels of turbulence away from the surface than both the shear-free or constant elasticity boundary condition.

Finally, we note that one of the long term goals of this research is to relate subsurface hydrodynamics, namely the velocity field, to observations that can be made of the water surface. Specifically, we are interested in utilizing remotely sensed imagery such as IR imagery and correlating this imagery to what is occurring beneath the water surface. The work of Saylor *et al.*[23,24,26] has demonstrated that infrared imagery is highly sensitive to the presence of surfactant monolayers and to the surface heat flux during evaporative convection. The sensitivity of IR imagery to the state of the water during evaporative convection suggests that information concerning subsurface hydrodynamics may be obtained remotely. The current study does not directly correlate infrared imagery of the water surface to subsurface hydrodynamics. However, the variation in velocity profiles as a function of surfactant contamination and as a function of heat flux, may be coupled with the work of Saylor *et al.* to provide a rough correlation between IR imagery and subsurface velocity characteristics. Future work where simultaneous measurements of surface imagery and subsurface profiles are obtained will permit more direct correlations.

ACKNOWLEDGMENTS

Financial support from the Office of Naval Research through the United States Naval Academy and the Naval Research Laboratory, is gratefully acknowledged. The authors would like to thank R. J. Adrian and A. K. Prasad for providing the data used for a comparison to the current results.

[1] S. Petterssen, *Introduction to Meteorology*, 3rd ed. (McGraw-Hill, New York, 1969).
[2] D. B. Thomas and A. A. Townsend, ''Turbulent convection over a heated horizontal surface,'' J. Fluid Mech. **2**, 473 (1957).
[3] A. A. Townsend, ''Temperature fluctuations over a heated horizontal surface,'' J. Fluid Mech. **5**, 209 (1959).
[4] R. J. Adrian, R. T. D. S. Ferreira, and T. Boberg, ''Turbulent thermal convection in wide horizontal fluid layers,'' Exp. Fluids **4**, 121 (1986).
[5] J. W. Deardorff and G. E. Willis, ''Investigation of turbulent thermal convection between horizontal plates,'' J. Fluid Mech. **28**, 675 (1967).
[6] J. C. Wyngaard, O. R. Cot'e, and Y. Izumi, ''Local free convection, similarity, and the budgets of shear stress and heat flux,'' J. Atmos. Sci. **28**, 1171 (1971).
[7] Z. Sorbjan, ''Similarity scales and universal profiles of statistical moments in the convective boundary layer,'' J. Appl. Meteorol. **29**, 762 (1990).
[8] W. G. Spangenberg and W. R. Rowland, ''Convective circulation in water induced by evaporative cooling,'' Phys. Fluids **4**, 743 (1961).
[9] K. B. Katsaros, W. T. Liu, J. A. Businger, and J. E. Tillman, ''Heat transport and thermal structure in the interfacial boundary layer measured in an open tank of water in turbulent free convection,'' J. Fluid Mech. **83**, 311 (1977).
[10] Y. L. Chernous'ko, ''Laboratory investigation of microconvection,'' Atmos. Oceanic Phys. **7**, 1096 (1971).
[11] B. F. Sharpley and L. M. K. Boelter, ''Evaporation of water into quiet air from a one-foot diameter surface,'' Ind. Eng. Chem. **30**, 1125 (1938).
[12] L. M. K. Boelter, H. S. Gordon, and B. F. Sharpley, ''Free evaporation into air of water from a free horizontal quiet surface,'' Ind. Eng. Chem. **38**, 596 (1946).
[13] E. M. Sparrow, G. K. Kratz, and M. J. Schuerger, ''Evaporation of water from a horizontal surface by natural convection,'' J. Heat Transfer **105**, 469 (1983).
[14] A. T. Prata and E. M. Sparrow, ''Forced convection evaporation from a cavity containing a liquid whose surface is curved by capillarity: computations in interlocking rectangular and cylindrical domains,'' Numer. Heat Transfer **8**, 667 (1985).
[15] A. T. Prata and E. M. Sparrow, ''Evaporation of water from a partially filled, cylindrical container to a forced convection air flow,'' Int. J. Heat Mass Transf. **29**, 539 (1986).
[16] G. A. Nunez and E. M. Sparrow, ''Models and solutions for isothermal and non-isothermal evaporation from a partially filled tube,'' Int. J. Heat Mass Transf. **31**, 461 (1988).
[17] E. M. Sparrow and G. A. Nunez, ''Experiments on isothermal and non-isothermal evaporation from partially filled, open-topped vertical tubes,'' Int. J. Heat Mass Transf. **31**, 1345 (1988).
[18] R. J. Volino and G. B. Smith, ''Use of simultaneous IR temperature measurements and DPIV to investigate thermal plumes in a thick layer cooled from above,'' Exp. Fluids **27**, 70 (1999).
[19] J. R. Saylor, ''Determining liquid substrate cleanliness using infrared imaging,'' Rev. Sci. Instrum. (to be published).
[20] N. L. Jarvis, ''The effect of monomolecular films on surface temperature and convective motion at the water/air interface,'' J. Colloid Sci. **17**, 512 (1962).
[21] K. B. Katsaros and W. D. Garrett, ''Effects of organic surface films on evaporation and thermal structure of water in free and forced convection,'' Int. J. Heat Mass Transf. **25**, 1661 (1982).
[22] W. M. Barger, ''A review of experimental observations and remaining questions concerning formation, persistence, and disappearance of sea slick,'' NRL Report 9313, 1991.
[23] J. R. Saylor, G. B. Smith, and K. A. Flack, ''The effect of a surfactant monolayer on the temperature field of a water surface undergoing evaporation,'' Int. J. Heat Mass Transf. **43**, 3073 (2000).
[24] J. R. Saylor, G. B. Smith, and K. A. Flack, ''An experimental investigation of the surface temperature field during evaporative convection,'' Phys. Fluids **13**, 428 (2001).
[25] A. K. Prasad and P. V. Gonuguntla, ''Turbulence measurements in non-penetrative thermal convection,'' Phys. Fluids **8**, 2460 (1996).
[26] J. R. Saylor, G. B. Smith, and K. A. Flack, ''Infrared imaging of the surface temperature field of water during film spreading,'' Phys. Fluids **12**, 597 (2000).